NASA/TM-2003-210742

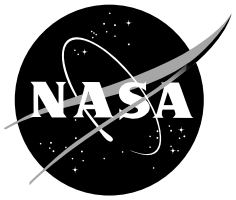

Experimental Evaluation of Hot Films on Ceramic Substrates for Skin-Friction Measurement

Gregory K. Noffz
NASA Dryden Flight Research Center
Edwards, California

Adrienne S. Lavine
University of California, Los Angeles
Los Angeles, California

Philip J. Hamory
NASA Dryden Flight Research Center
Edwards, California

March 2003

The NASA STI Program Office…in Profile

Since its founding, NASA has been dedicated to the advancement of aeronautics and space science. The NASA Scientific and Technical Information (STI) Program Office plays a key part in helping NASA maintain this important role.

The NASA STI Program Office is operated by Langley Research Center, the lead center for NASA's scientific and technical information. The NASA STI Program Office provides access to the NASA STI Database, the largest collection of aeronautical and space science STI in the world. The Program Office is also NASA's institutional mechanism for disseminating the results of its research and development activities. These results are published by NASA in the NASA STI Report Series, which includes the following report types:

- TECHNICAL PUBLICATION. Reports of completed research or a major significant phase of research that present the results of NASA programs and include extensive data or theoretical analysis. Includes compilations of significant scientific and technical data and information deemed to be of continuing reference value. NASA's counterpart of peer-reviewed formal professional papers but has less stringent limitations on manuscript length and extent of graphic presentations.

- TECHNICAL MEMORANDUM. Scientific and technical findings that are preliminary or of specialized interest, e.g., quick release reports, working papers, and bibliographies that contain minimal annotation. Does not contain extensive analysis.

- CONTRACTOR REPORT. Scientific and technical findings by NASA-sponsored contractors and grantees.

- CONFERENCE PUBLICATION. Collected papers from scientific and technical conferences, symposia, seminars, or other meetings sponsored or cosponsored by NASA.

- SPECIAL PUBLICATION. Scientific, technical, or historical information from NASA programs, projects, and mission, often concerned with subjects having substantial public interest.

- TECHNICAL TRANSLATION. English-language translations of foreign scientific and technical material pertinent to NASA's mission.

Specialized services that complement the STI Program Office's diverse offerings include creating custom thesauri, building customized databases, organizing and publishing research results…even providing videos.

For more information about the NASA STI Program Office, see the following:

- Access the NASA STI Program Home Page at ***http://www.sti.nasa.gov***

- E-mail your question via the Internet to help@sti.nasa.gov

- Fax your question to the NASA Access Help Desk at (301) 621-0134

- Telephone the NASA Access Help Desk at (301) 621-0390

- Write to:
  NASA Access Help Desk
  NASA Center for AeroSpace Information
  7121 Standard Drive
  Hanover, MD 21076-1320

NASA/TM-2003-210742

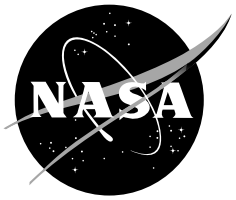

Experimental Evaluation of Hot Films on Ceramic Substrates for Skin-Friction Measurement

Gregory K. Noffz
NASA Dryden Flight Research Center
Edwards, California

Adrienne S. Lavine
University of California, Los Angeles
Los Angeles, California

Philip J. Hamory
NASA Dryden Flight Research Center
Edwards, California

National Aeronautics and
Space Administration

Dryden Flight Research Center
Edwards, California 93523-0273

March 2003

NOTICE

Use of trade names or names of manufacturers in this document does not constitute an official endorsement of such products or manufacturers, either expressed or implied, by the National Aeronautics and Space Administration.

Available from the following:

NASA Center for AeroSpace Information (CASI)
7121 Standard Drive
Hanover, MD 21076-1320
(301) 621-0390

National Technical Information Service (NTIS)
5285 Port Royal Road
Springfield, VA 22161-2171
(703) 487-4650

ABSTRACT

An investigation has been performed on the use of low-thermal conductivity, ceramic substrates for hot films intended to measure skin friction. Hot films were deposited on two types of ceramic substrates. Four hot films used composite-ceramic substrates with subsurface thermocouples (TCs), and two hot films were deposited on thin Macor® substrates. All six sensors were tested side by side in the wall of the NASA Glenn Research Center 8-ft by 6-ft Supersonic Wind Tunnel (SWT). Data were obtained from zero flow to Mach 1.98 in air. Control measurements were made with three Preston tubes and two boundary-layer rakes. The tests were repeated at two different hot film power levels. All hot films and subsurface TCs functioned throughout the three days of testing. At zero flow, the films on the high-thermal conductivity Macor® substrates required approximately twice the power as those on the composite-ceramic substrates. Skin-friction results were consistent with the control measurements. Estimates of the conduction heat losses were made using the embedded TCs but were hampered by variability in coating thicknesses and TC locations.

NOMENCLATURE

Acronyms

APSO	adjustable-protrusion surface-obstacle
BL	boundary layer
HRSI	high-temperature reusable surface insulation
NASA	National Aeronautics and Space Administration
RCG	reaction cured glass
RTD	resistance temperature detector
SWT	8-ft by 6-ft Supersonic Wind Tunnel
TC	thermocouple

Symbols

A	calibration constant slope, $(\rho_w \tau_w)^{1/3}/(I^2 R/\Delta T)$
B	calibration constant offset, $(\rho_w \tau_w)^{1/3}$
C_p	specific heat, J/kgK
I	hot film current, amps
k	thermal conductivity, W/mK
R	electrical resistance, Ω
t	time, sec
T	temperature, K
α	thermal diffusivity, m^2/s

ΔT	temperature difference between film and fluid, K
ρ	density, kg/m^3
τ_w	wall shear stress, N/m^2
μ	dynamic viscosity, kg/ms
$\perp$	perpendicular

Subscripts

f	fluid property
s	substrate property
w	wall property

INTRODUCTION

Measuring skin friction on the surfaces of wind tunnel models, aircraft, watercraft, and other vehicles is crucial to validating computational fluid dynamics and boundary-layer codes. Skin-friction measurement is also crucial to characterizing the effectiveness of skin-friction reduction schemes. Accurate skin-friction measurements are generally more difficult to attain than more fundamental flow measurements such as pressure and temperature. The available methods of skin-friction measurement include floating-element gages,[1,2,3,4] total pressure rakes to determine boundary-layer profiles,[5] Stanton gages or Preston tubes to measure the difference between total and static pressure at the surface,[6,7] the observation of oil flow on the surface,[8] and surface-mounted hot films.[9,10,11] Of these methods, floating-element gages are the most direct method of measurement, but they still require a static calibration. All other methods are indirect and require some type of flow calibration or analysis. These calibrations are usually dependent on flow conditions (that is, Reynolds number, laminar as opposed to turbulent, subsonic as opposed to supersonic). Supplementary measurements often are required to determine the flow condition and then determine the calibration to use.

Hot film sensors, consisting of a metallic film on an electrically nonconducting substrate, have been used to measure skin friction as early as 1931.[12] The film is kept at a fixed elevated temperature relative to that of the local flow, and the required electrical power is measured. The rate of heat transfer to the flow is related to the velocity gradient at the surface, which in turn is related to the skin friction. Because of their small thermal mass, hot films quickly respond to fluctuations in the local flow and thus are used to determine flow direction (with multiple hot films) and local flow regime (laminar, transitional, or turbulent). Fabricating hot film substrates from low-thermal conductivity ceramics serves to decrease heat conduction to the substrate. Furthermore, the layered nature of the fabrication allows the installation of thermocouple (TC) junctions underneath the hot film, which can provide additional information on the conduction heat loss.

When the hot film is used to measure skin friction, the heat supplied to maintain an elevated temperature is related to skin friction by a variety of calibrations stemming from both experiment and analysis. Most are of the following form[13]

$$(\rho_w \tau_w)^{1/3} = A\left(\frac{I^2 R}{\Delta T}\right) - B \quad (1)$$

where ΔT is the temperature difference between the film and the fluid. The information available from the hot film anemometry is the total heat dissipated from the film (I^2R). This information includes not only heat transferred directly to the fluid, but also heat conducted to the substrate accounted for by *B* in eq. 1. The distance the heat penetrates into the substrate increases with increasing substrate conductivity. Any substrate will allow some heat to conduct parallel to the surface before it is removed by the fluid, thus increasing the "effective length" of the hot film in the streamwise direction. The parameter *A* varies inversely with the effective length.[13,14] Thus, a hot film substrate with a high-thermal conductivity will have lower sensitivity (lower *A*) and a larger conduction heat loss (larger *B*). All hot film skin-friction measurements must overcome this complication. The use of a low-thermal conductivity substrate can reduce *B* and increase *A*, making the hot film more sensitive to changes in skin friction.

This research investigates the possible advantages of using low-thermal conductivity ceramics for hot film substrates. Hot films were deposited on two types of ceramic substrates. The first is a homogeneous substrate fabricated from Macor® (Corning, Inc., Corning, New York), a commercially available, machinable ceramic. The second is a composite-ceramic substrate composed of high-temperature reusable surface insulation (HRSI), a porous, low-density (ρ = 352 kg/m^3) ceramic, and coated with reaction cured glass (RCG), a high-density, nonporous glass. The RCG provides a tough exterior, and the composite nature of the substrate allows for the installation of small TCs under the coating. The TCs are positioned under the hot film and potentially can be used to estimate conduction heat loss. The ceramic substrates will reduce the conduction heat loss, hopefully leading to increased sensitivity and a gage better suited for measuring changes in skin friction.

A previous report[15] documented conjugate heat transfer studies of hot films on composite-ceramic, Macor®, and quartz substrates. Time step constraints prevented modeling of the high-speed flows seen in the tunnel experiment described in the succeeding paragraphs; however, the modeling that was done confirmed the trend toward smaller film effective lengths with decreasing thermal conductivity. The thermal properties are presented in the next section.

This report presents results from the hot film tests conducted in the NASA Glenn Research Center (Cleveland, Ohio) 8-ft by 6-ft Supersonic Wind Tunnel (SWT). Data from zero flow to Mach 1.98 in air were obtained and repeated (for some of the films) at different hot film overheats.

SENSOR DESCRIPTION

The composite-ceramic substrate is a cylinder, 12.70 mm in diameter and 15.88 mm long. Figure 1 shows a cross-sectional view. The RCG coating (approximately 0.127 mm thick) extends over the face of the cylinder and approximately one-third of the way down the sides, thus providing a surface on which the metallic hot film can be deposited. Figure 2 shows one of the hot film sensors (designated "CC1") on a composite-ceramic substrate. The sensor is potted into the white Macor® sleeve. The RCG coating is so thin that the three TC junctions are visible underneath. The hot film runs perpendicular to the lands of the TCs, and the hot film leads run down the sides of the substrate to the end of the RCG coating. Small gage wires are attached to the end of the leads with electrically conductive epoxy.

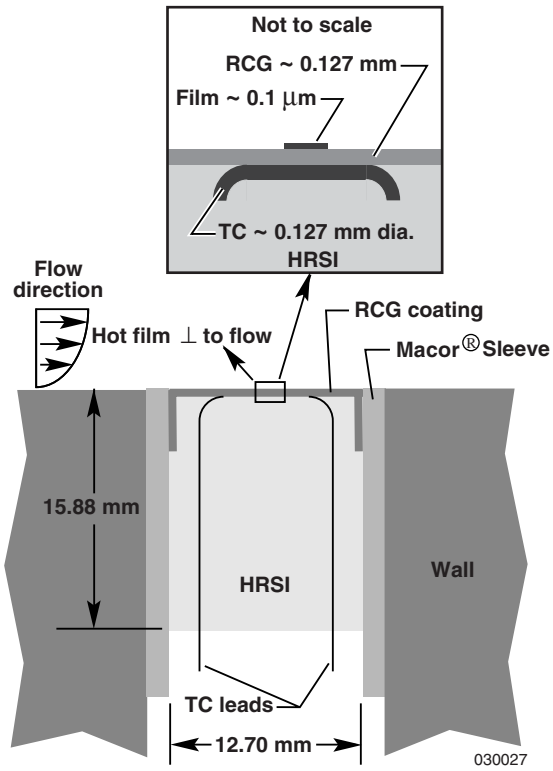

Figure 1. Cross section of composite-ceramic hot film.

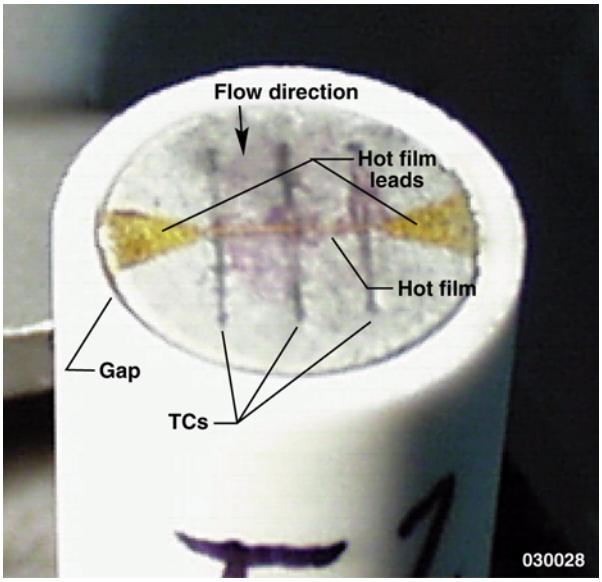

Figure 2. Hot film on composite-ceramic substrate.

On one of the composite-ceramic sensors (designated “CC2”), the hot film was deposited parallel to the TCs and directly over the center TC. Because the hot film is positioned over the entire land of the center TC, conduction heat loss down the leads of the TC is minimized and offers an interesting comparison with the TCs that are oriented perpendicular to the films. For all of the composite-ceramic substrates, the RCG coating (and thus, the hot film leads) terminate about one-third of the way down the side of the cylinder, and wires must be routed up between the Macor® sleeve and the substrate. This arrangement leaves a small gap that must be filled prior to testing (fig. 2).

Figure 3 shows a cross section of the Macor® hot film substrate. The additional strength and machinability of the Macor® allow the substrate to be hollowed out, limiting the conduction path away from the surface. For all of the Macor® substrates, the hot film leads were deposited all the way down the sides of the cylinders. A shorter sleeve is then used, leaving the leads exposed and allowing the wire connections to be made “out in the open,” thus eliminating the sleeve-substrate gap. Unlike the composite-ceramic substrates, no filler was required for the all-Macor® sensors (fig. 4).

Table 1 compares the thermal properties of the substrate materials in which the significantly lower thermal conductivity, k, of the HRSI ceramic (the primary constituent of the composite-ceramic substrate) is evident. Fluid-substrate material property ratios, important parameters in conjugate heat transfer problems,[16] are also provided.

Table 1. Substrate material properties and air/substrate material property ratios (300 K, 1 atm).

Property	HRSI	RCG	Macor®	Quartz	Air
ρ	352	1666	2516	2650	1.177
C_p	712	852	796	815	1005
k	0.081	0.917	1.39	9	0.0267
α_f/α_s	69.8	34.9	32.5	5.4	
k_f/k_s	0.329	0.029	0.019	0.003	

The hot film and leads are deposited using organo-metallics, which are essentially heavy metals in solution with organic solvents. Both the hot film and leads are a gold alloy. The surface of the Macor® substrate is smooth enough that photolithography techniques can be employed. The surface of the composite-ceramic substrate is irregular enough that the film and leads had to be painted on using carbon fiber brushes. After the organo-metallics are applied, the substrates are heated to dissipate the organics, leaving only the metal. The gold leads are relatively wide (approximately 4.76 mm or 3/16 in.) and neck-down to the film, which is approximately 0.16 mm (0.006 in.) wide. Most of the electrical resistance is in the film, similar to the filament of a light bulb. Optically measured film dimensions are listed in table 2. Films with composite-ceramic substrates are designated “CC1-4,” and the all-Macor® sensors are designated “M1-2.”

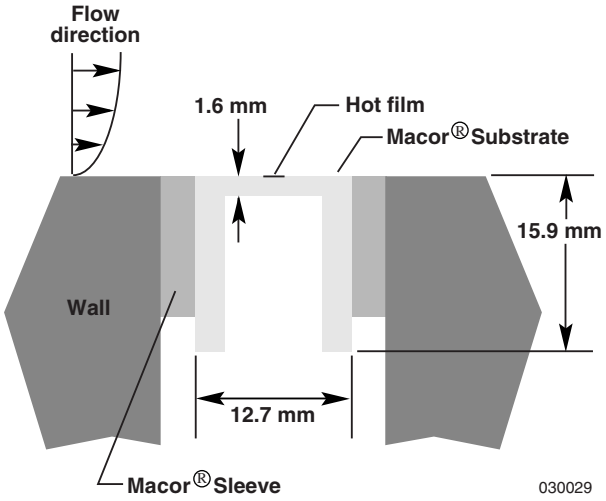

Figure 3. Cross section of Macor® hot film substrate.

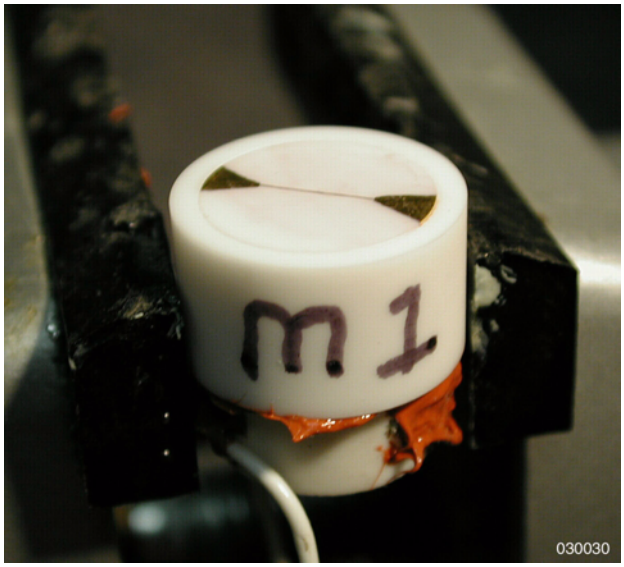

Figure 4. Macor® hot film sensor.

Table 2. Hot film dimensions (in mm or sq. mm) and nominal resistances (Ohms).

Sensor	Width	Length	Area	Resistance	TC Configuration
CC1	0.16	6.35	1.016	26.2	Perpendicular
CC2	0.16	5.92	0.947	10.38	Parallel
CC3	0.152	5.84	0.8877	10.89	Perpendicular
CC4	0.17	6.02	1.0234	9.98	Perpendicular
M1	0.091	6.35	0.578	37.4	N/A
M2	0.11	6.02	0.662	28.07	N/A

All six hot film sensors were heated with temperature-compensated, constant temperature anemometers.[17] These anemometers work like standard constant temperature anemometers but use a temperature feedback to adjust the film temperature should ambient conditions change. In this case, the anemometers operate more like constant-overheat anemometers. The following modifications were made to the anemometers to meet the specific requirements of this experiment:

1. The voltage at the hot film was measured, in addition to the standard anemometer bridge voltage output, to derive the temperature of the hot film and the power dissipated.

2. Bridge ratios ranging from 9 to 16 (higher than the standard ratio of 5) were used to reduce self-heating errors in the platinum ambient-temperature-sensing resistance temperature detectors (RTDs).

TUNNEL DESCRIPTION

Soeder[18] describes the NASA Glenn SWT complex. The SWT is an atmospheric tunnel capable of Mach numbers from 0.0 to 0.1, and from 0.25 to 2.0. It can be run in an open-loop mode for propulsion tests, or, as in the case of these experiments, in a closed-loop, aerodynamic mode. Hydraulically actuated, flexible nozzle walls along with three 29,000-hp (21,625 kW) electric motors control the test section Mach number. The upstream portion (approximately 3 m) of the test section has solid walls for supersonic testing, and the aft portion (approximately 4.4 m) has porous walls that absorb shocks for transonic testing. An activated alumina pebble bed can provide about 1000 kg/sec of dried atmospheric air for approximately one hour.

EXPERIMENT DESCRIPTION

The hot film experiment “piggybacked” on a standard tunnel calibration test alongside an adjustable-protrusion surface-obstacle (APSO) skin-friction vector gage[19] and various sensors used to obtain control measurements. The tunnel calibration consists of measuring surface pressures on a nonmoving, sting-mounted cone while the tunnel is run throughout the Mach range. The hot films, APSO

gage, and control sensors were mounted on a flush, 76.2-cm by 30.5-cm panel well upstream of the calibration cone and sting. Flow over the test panel was always turbulent. Results from the APSO gage are reported in ref. 19.

Figure 5a shows a diagram of the sensor locations on the panel. The figure also depicts the hot film and TC orientation, in addition to the relative position of the sensors. The hot films, which are always perpendicular to the flow direction, are drawn as heavy lines on the faces of the substrates. The thinner lines are the subsurface TCs. For hot film CC2, T_{fore} and T_{aft} are the temperatures from the upstream and downstream TCs, respectively. For hot films CC1, CC3, and CC4, T_{left} and T_{right} are defined as such while looking into the flow direction.

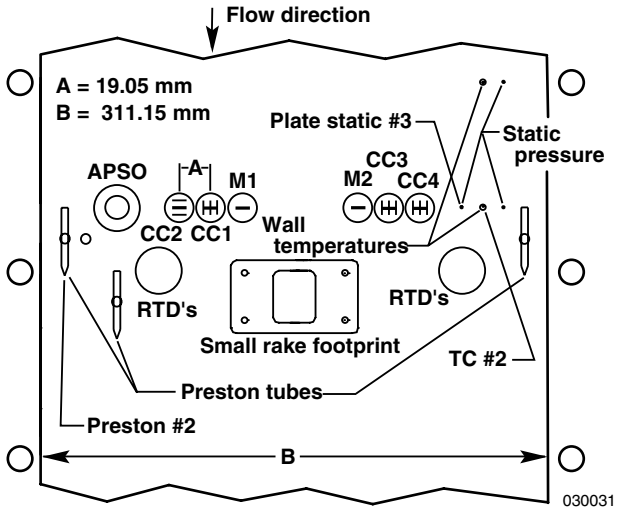

(a) Instrumentation layout.

Figure 5. Sensor panel.

Figure 5b shows the panel with the straight rake installed. The hot film substrates occupy 15.88 mm holes centered 19.05 mm apart. The hot film substrates are centered about the plate centerline with the two all-Macor® sensors at the interior positions. Sensor CC2, the composite-ceramic sensor with the TCs aligned with the hot film (perpendicular to the flow), occupies the left-most position. The APSO gage (shown partially deployed in figure 5b) is on the left flank. The boundary-layer rake is mounted on the plate centerline aft of the row of hot films, but the approach from upstream is unobstructed. Outboard and aft of the hot film row are two alumina substrates, which support the RTDs that provide temperature feedback for the anemometers. The two most outboard positions are occupied by two Preston tubes. A third Preston tube is located aft of the APSO gage and gives valid results only when the APSO gage is flush.

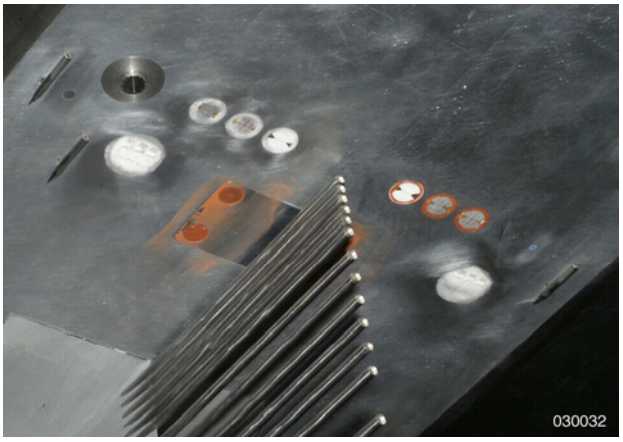

(b) Sensor suite with large rake.

Figure 5. Concluded.

Two boundary-layer rakes were used for the tests. The first was a curved rake designed for a high density of measurements near the surface and originally calibrated in this tunnel.[20] This rake, however, was not tall enough to span the entire boundary layer, so the curved rake was replaced by a taller, straight rake (shown in figure 5b), and testing was repeated the following day. The method was the same as the method[20] used for the original curved rake calibration.

Various auxiliary measurements were made, including two wall temperatures (figs. 5a and 5b), three static pressures (fig. 5a), and several static pressures on the tunnel walls away from the panel. The wall temperature sensors consisted of bulb TCs potted in epoxy, and the epoxy and TCs were sanded flat with the wall. The result was a flush installation with the bare metal of the TCs exposed to the flow.

One tunnel run was made each evening from December 4 to December 6, 2001. A tunnel run consisted of running at Mach 0.5 for a short period of time, proceeding to maximum Mach, and then stepping down to zero in approximately 0.1 Mach steps. After the tunnel stabilized at each desired Mach number, the APSO gage was deployed and retracted over several minutes. During this time, hot film voltages and subsurface TC data were recorded at 5 samples per sec. Tunnel wall static pressures, plate static pressures, rake pressures, Preston tube pressures, and wall temperatures were recorded by the SWT "ESCORT" data system.[18] All data presented are from the December 5 and 6 runs.

RESULTS AND DATA ANALYSIS

Between the December 5 and 6 runs, the anemometry circuits, designed for much smaller films, were exceeding the current limits of the amplifiers. To get response out to higher Mach numbers, the overheat was lowered on sensors CC2 through CC4 by approximately one-third (from the 90–100 °C range to the 60–70 °C range). Not enough hardware was available to reduce the overheat of the remaining sensors.

Tables 3a and 3b show selected zero-flow results from the December 5 and 6 runs, respectively. The roughly 5-percent drop in overheat ratio reduces zero-flow power consumption by approximately one-third. Film temperatures drop by about 33 °C. In the case of the subsurface TCs that are oriented

perpendicular to the films (CC1, CC3, and CC4), T_{center} is always higher as expected, because the films are losing heat through the film leads. In the case of CC2 where the center TC is aligned under the film, T_{center} is much higher than those of the other films, even though the film temperatures are comparable (at the same overheat). The higher temperature indicates that for the perpendicular TCs, heat is also being lost through the TC leads, resulting in a lower indicated temperature. The T_{fore} and T_{aft} on sensor CC2 are not under any part of the film, yet they are about 30 °C warmer than ambient (at the higher overheat). Table 3b shows that the power dissipated from sensor M1 also changed from the 5th of December to the 6th. The reason for this change is not understood. The overheat was not changed, so the power dissipated should not have changed either. The $T_{ambient}$ was approximately 25 °C on December 5 and approximately 22 °C on December 6.

Table 3a. Zero-flow hot film temperatures, December 5 run. Temperatures in °C.

	CC1	CC2	CC3	CC4	M1	M2
Power, W	0.18	0.3	0.24	0.22	0.61	0.56
T_{film}	118	128	125	121	126	120
T_{left}	62		79	63		
T_{center}	77	106	81	79		
T_{right}	63		73	76		
T_{fore}		54				
T_{aft}		58				

Table 3b. Zero-flow hot film temperatures, December 6 run. Temperatures in °C.

	CC1	CC2*	CC3*	CC4*	M1	M2
Power, W	0.18	0.2	0.17	0.15	0.47	0.55
T_{film}	117	94	92	89	125	116
T_{left}	61		64	52		
T_{center}	75	79	64	52		
T_{right}	62		59	59		
T_{fore}		46				
T_{aft}		47				

*Overheat reduced from approximately 1.22 to approximately 1.16 from December 5.

Figures 6, 7, and 8 show relevant tunnel parameters as a function of time for the December 6 run. The tunnel was operating for approximately 3 hours and 45 minutes. Tunnel data were not recorded between steady-state Mach numbers, resulting in gaps in the time histories (figs. 6–9). The data has been considerably thinned to distinguish the symbols. Hot film parameters were recorded continuously. Tunnel wall temperature peaked just over 60 °C at the maximum Mach number of just under 2. Tunnel total temperature peaked at about 85 °C and managed to achieve near-steady-state conditions at each test point, whereas wall temperature was usually changing throughout the test points. Density decreases with increasing Mach number down to about 20 percent of atmospheric density (fig. 8). The density is calculated based on wall temperature and boundary layer (BL) edge pressure.

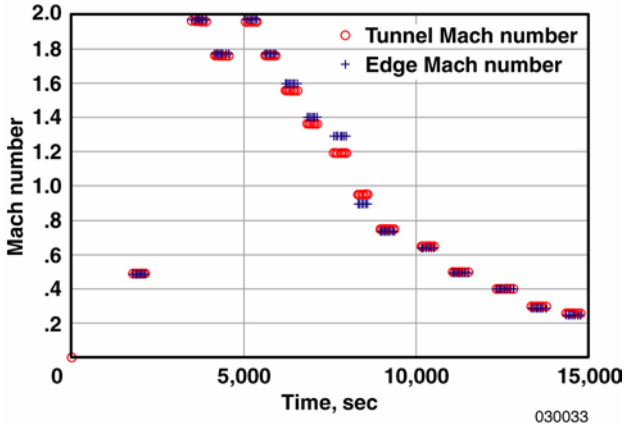

Figure 6. Tunnel and BL edge Mach numbers.

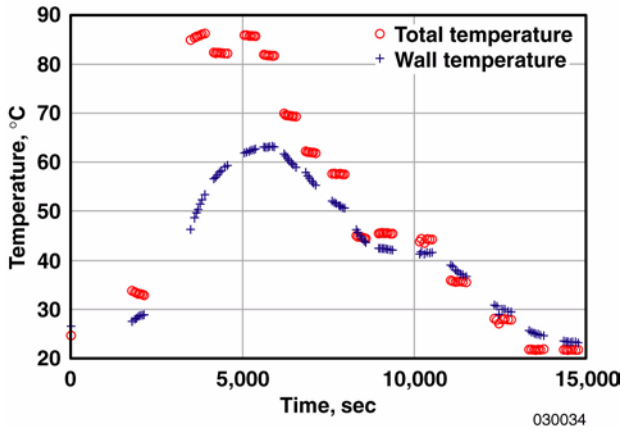

Figure 7. Tunnel total and wall temperatures.

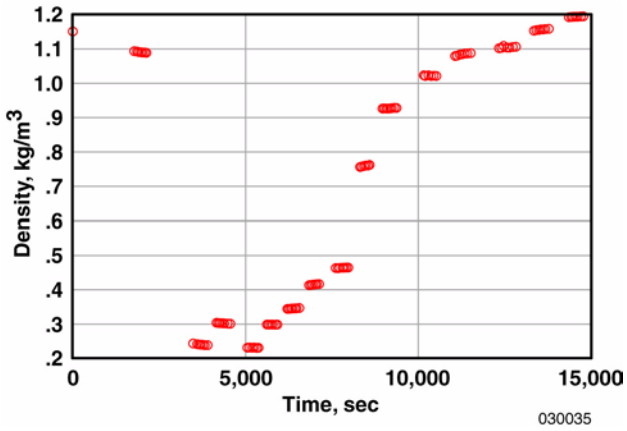

Figure 8. Density based on wall temperature and BL edge pressure.

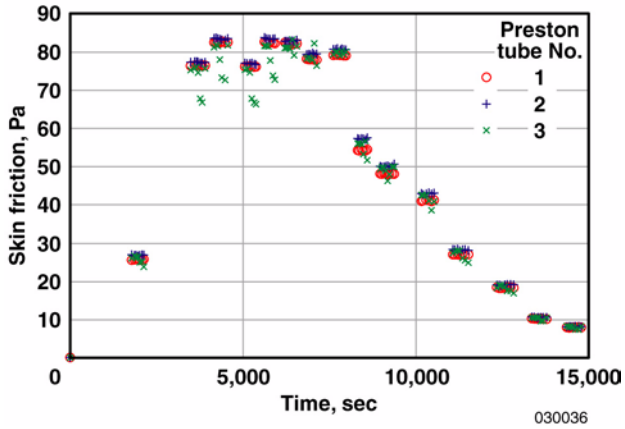

Figure 9. Preston tube skin frictions.

Preston tube data were reduced using the Allen[6] correction to the method of Bradshaw and Unsworth.[21] This method used TC #2 for wall temperature and BL edge pressure for the reference pressure. The resulting skin frictions are plotted in figure 9. Using the same approach, reference 20 found Preston tube skin-friction measurements to be within ±5 percent of theory.

Preston tube 3 is located downstream of the APSO gage, so when the APSO is deployed during the test point, data from this Preston tube should be disregarded. Preston tube 1 is located to the left of the APSO (fig. 5a) and generally gives lower skin-friction values than does Preston tube 2, located on the cleaner right side of the panel. Data from Preston tube 2 are used as calibration points for the hot films. Note that maximum skin friction is exerted on the panel at Mach 1.77, not at Mach 1.98, because density decreases with increasing Mach number in the SWT.

All hot film data were calibrated to Preston tube 2, but different Mach points were chosen for various films, because some films were saturated at the higher values of $(\rho_w \tau_w)^{1/3}$ (CC2 in figure 11 and M2 in

figure 15). Hot films CC1 and CC3 both were calibrated at Mach 0.9 and 0.25; CC2 and M2 both were calibrated at Mach 1.8 and 0.25; and CC4 and M1 both were calibrated at Mach 0.4 and 0.25. Slopes and offsets (*A* and *B* for eq. 1) were calculated, and the results are compared in figures 10–15. The points used in these figures are averages from 40 sec of data taken during the middle of each test point.

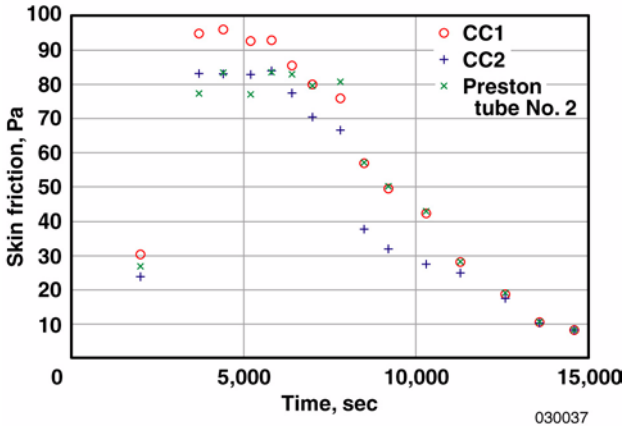

Figure 10. Hot films CC1, CC2, and Preston tube 2 skin frictions.

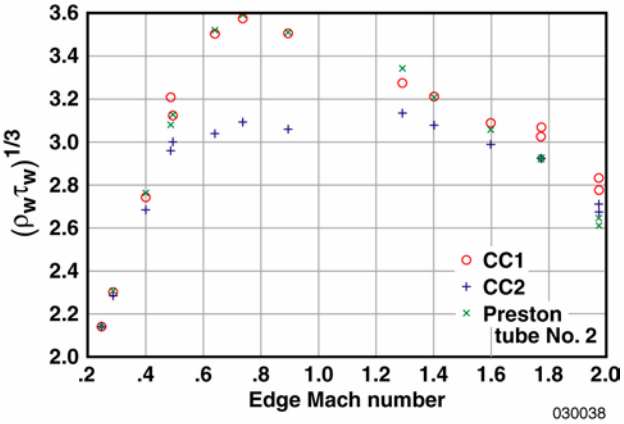

Figure 11. Hot films CC1, CC2, and Preston tube 2 skin-friction density products.

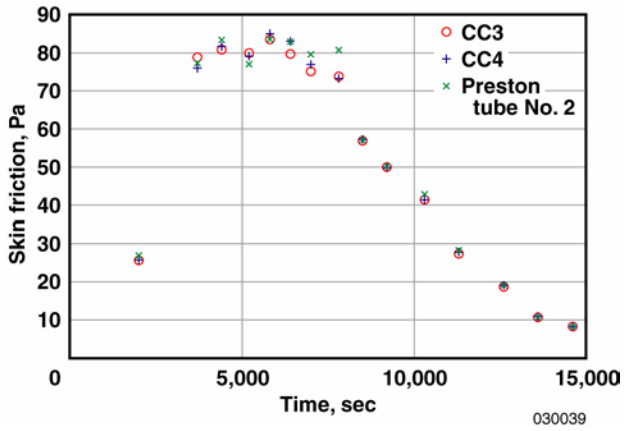

Figure 12. Hot films CC3, CC4, and Preston tube 2 skin frictions.

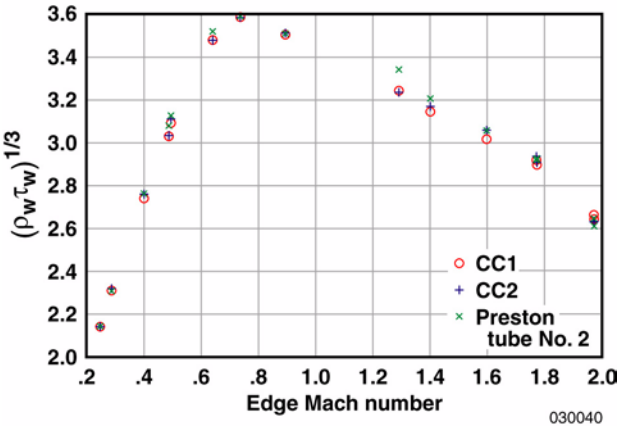

Figure 13. Hot films CC3, CC4, and Preston tube 2 skin-friction density products.

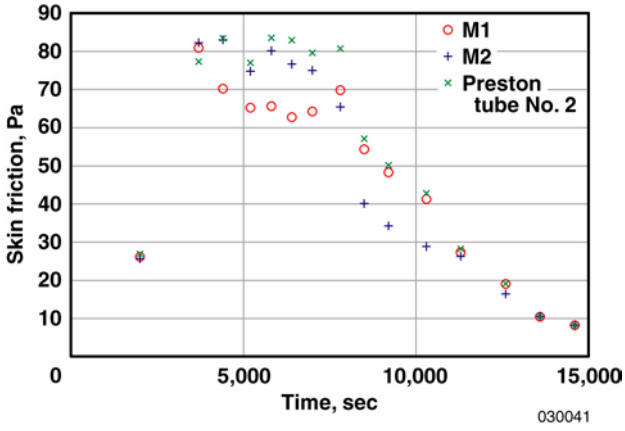

Figure 14. Hot films M1, M2, and Preston tube 2 skin frictions.

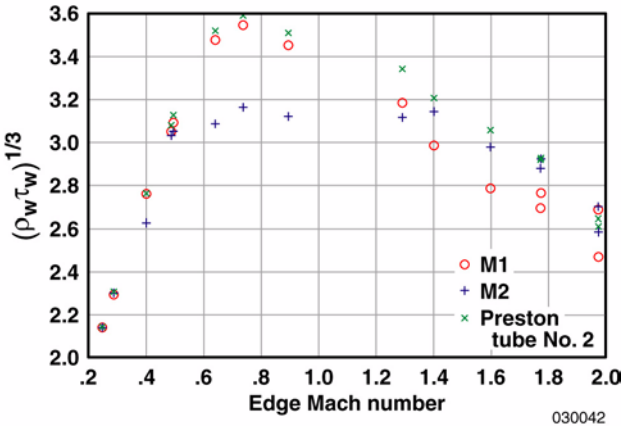

Figure 15. Hot films M1, M2, and Preston tube 2 skin-friction density products.

Hot film CC1 shows good agreement at subsonic Mach numbers (t>8,000 sec and t=2,000 sec) but overpredicts skin friction at supersonic Mach numbers. Hot film CC1 overpredicts by about 14–19 percent. Hot film CC2 matches well at low Mach numbers (t>12,000 sec) and matches better than CC1 at higher Mach numbers, but the current amplifier is saturated (fig. 11) at the high values of $(\rho_w \tau_w)^{1/3}$. Hot films CC3 and CC4, located on the right side of the panel opposite the APSO, agree much better with the Preston tube at all the test points. Both CC3 and CC4 are within about 2.5 percent at supersonic Mach numbers and are usually closer elsewhere. Recall that the overheats on films CC2, CC3, and CC4 were lowered after the film amplifiers were believed to be saturating at the high values of $(\rho_w \tau_w)^{1/3}$, but figure 11 shows that CC2 is still saturating. Although less than perfect at the two highest Mach numbers, CC1 does not appear saturated and still follows the trends observed in Preston tube 2.

The films with Macor® substrates, M1 and M2, located opposite the centerline on each side of the rake, also match the Preston tube well at low subsonic points (t>12,000 sec). Hot film M2, however, was saturated at the high values of $(\rho_w \tau_w)^{1/3}$ (fig. 15). Hot film M1 underpredicts skin friction at supersonic Mach numbers, while M2 is closer.

Because the slope, *A*, in eq. 1 is inversely proportional to film area,[13] and the hot films tested here have different dimensions (table 2), *A* has to be normalized by film area prior to comparison. Table 4 shows the calibration constants multiplied by film area, offsets, and the non-normalized calibration constants. The calibration constants for all the films were calculated using the test points from Preston tube 2 noted previously. Note that the offsets (*B* in eq. 1) are larger for the high-thermal conductivity Macor® substrates, as expected.

Table 4. Hot film slopes and offsets.

	CC1	CC2	CC3	CC4	M1	M2
Slope, *A*	1431	826	1082	1046	1562	1230
A x area	1454	782	961	1071	903	814
Offset, *B*	3.028	2.639	3.047	2.599	7.494	7.347

Recall that hot films CC2, CC3, and CC4 were also running at a lower overheat (approximately 1.16 as opposed to 1.22), so one would expect CC1 to have a higher normalized sensitivity. Note that M1 and M2, in spite of operating at the higher overheat, have a lower normalized sensitivity than all of the films except for CC2. Unfortunately, manufacturing tolerances and differing overheats preclude getting the films on equal footing with respect to all variables, so direct comparisons are difficult to attain.

Figures 16–19 show the temperature time histories from the subsurface TCs in sensors CC1 through CC4. The data has been considerably thinned to distinguish the symbols. The temperature differences remain largely constant throughout the test. Because heat is conducted laterally from the films to the relatively cool leads, one would expect the outboard TCs to measure a lower temperature. Hot film CC1 (fig. 16) behaves as expected with the center TC remaining warmer throughout the test. The middle TC of CC2, aligned with the hot film, is generally about 15–20 °C higher than the middle TCs of the other composite-ceramic sensors, including CC1, even though CC1 operated at a higher overheat. The aft TC, downstream of the heat source, remains warmer than the upstream (“fore”) TC (fig. 17).

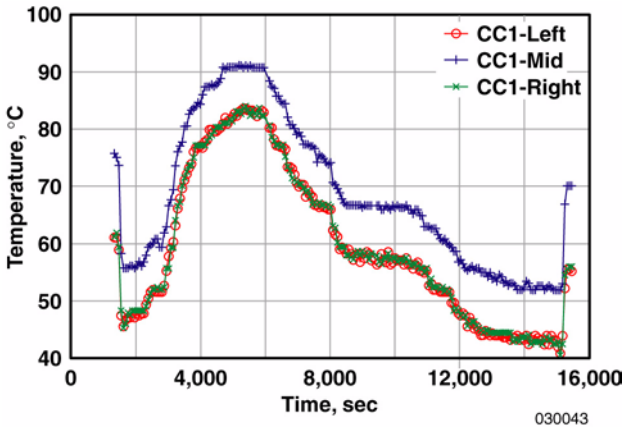

Figure 16. Hot film CC1 subsurface temperatures.

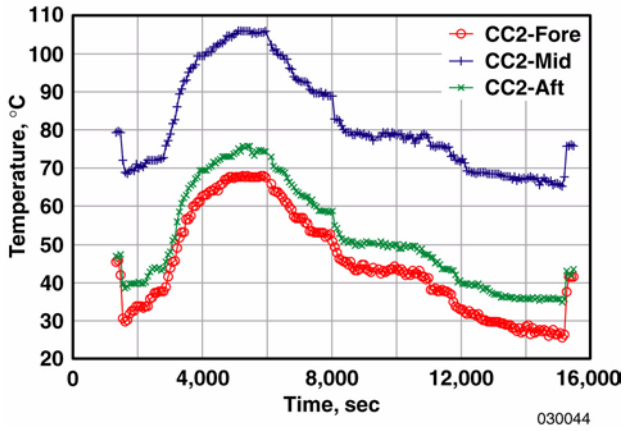

Figure 17. Hot film CC2 subsurface temperatures.

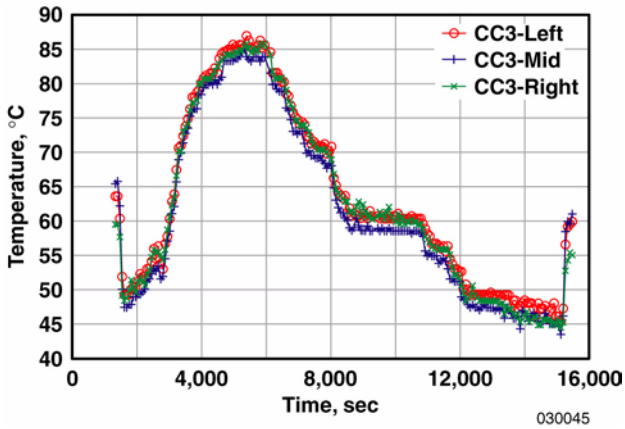

Figure 18. Hot film CC3 subsurface temperatures.

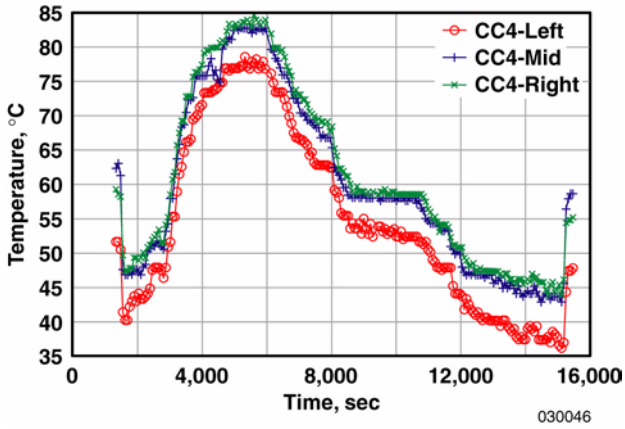

Figure 19. Hot film CC4 subsurface temperatures.

The middle TC temperature of CC3 is approximately equal to, yet lower than, the right and left TC temperatures, which probably reflects a nonuniform RCG coating thickness. Likewise, the right TC of CC4 is the warmest of the CC4 TCs throughout the test, indicating that the right TC is under a thinner RCG coating. Variations in coating thicknesses and uncertainties in the precise locations of the TC junctions create difficulty in estimating the conduction heat loss component for these particular prototypes. Nevertheless, improvements in packaging and coating control offer promise in this regard.

The higher temperature measured by the middle TC of CC2, relative to the middle TCs of the other composite-ceramic sensors, indicates that heat is being conducted away from the films through the TC wire, particularly in the case of CC1, CC3, and CC4 where the TC wire is perpendicular to the films. These additional conduction paths raise the issue of whether or not the presence of the TCs is helping to thwart the advantage of the low-thermal conductivity substrates. Testing another composite-ceramic hot film without subsurface TCs installed would have been enlightening, but none was fabricated for this test.

CONCLUSIONS

Four novel hot films on low-thermal conductivity ceramic substrates with subsurface TCs, along with two hot films on machinable ceramic substrates, were fabricated and tested in a supersonic wind tunnel. Skin-friction results from two of the hot films on low-thermal conductivity substrates matched the control measurement, from Mach 0.25 to nearly Mach 2, to within 3 percent. For the other two hot films on low-thermal conductivity substrates, packaging and tunnel integration shortcomings might have led to large discrepancies at supersonic Mach numbers; however, these sensors matched the control measurement better at subsonic points than at supersonic points. The hot films on low-thermal conductivity substrates showed lower zero-flow heat losses and offsets than those of the hot films on machinable ceramic substrates. The subsurface TCs in the low-thermal conductivity substrates were installed to estimate the conduction heat loss from the films. While the results are intriguing, coating tolerance and TC position uncertainties prevented conduction estimates from these prototypes.

REFERENCES

1. Frei, D. and H. Thomann, “Direct measurements of skin friction in a turbulent boundary layer with a strong adverse pressure gradient,” *Journal of Fluid Mechanics*, vol. 101, pt. 1, 1980, pp. 79–95.

2. Garringer, Darwin J. and Edwin J. Saltzman, *Flight Demonstration of a Skin-Friction Gage to a Local Mach Number of 4.9*, NASA TN D-3830, Feb. 1967.

3. Mabey, Dennis G. and Laurie Gaudet, “Performance of Small Skin Friction Balances at Supersonic Speeds,” *Journal of Aircraft*, vol. 12, no. 10, Oct. 1975, pp. 819–825.

4. Schmidt, Martin A., Roger T. Howe, Stephen D. Senturia, and Joseph H. Haritonidis, “Design and Calibration of a Microfabricated Floating-Element Shear-Stress Sensor,” *IEEE Transactions on Electron Devices*, vol. 35, no. 6, June 1988, pp. 750–757.

5. Clauser, Francis H., “Turbulent Boundary Layers in Adverse Pressure Gradients,” *Journal of Aeronautical Science*, vol. 21, no. 91, Feb. 1954, pp. 91–108.

6. Allen, Jerry M., *Reevaluation of Compressible-Flow Preston Tube Calibrations*, NASA TM X-3488, March 1977.

7. Preston, J.H., "The Determination of Turbulent Skin Friction by Means of Pitot Tubes," *Journal of the Royal Aeronautical Society*, vol. 58, no. 518, Feb. 1954, pp. 109–121.

8. Zilliac, Gregory G., *Further Developments of the Fringe-Imaging Skin-Friction Technique*, NASA TM 110425, Dec. 1996.

9. Liepmann, H.W. and G.T. Skinner, *Shearing-Stress Measurements by Use of a Heated Element*, NACA TN 3268, 1954.

10. Ludwieg, H., *Instrument for Measuring the Wall Shearing Stress of Turbulent Boundary Layers*, NACA TM 1284, 1950.

11. Ludwieg, H. and W. Tillmann, *Investigations of the Wall-Shearing Stress in Turbulent Boundary Layers*, NACA TM 1285, May 1950.

12. Fage, A. and V.M. Falkner, "On the Relation Between Heat Transfer and Surface Friction for Laminar Flow," *Aeronautical Research Council R&M No. 1408*, London, 1931.

13. Hanratty, Thomas J. and Jay A. Campbell, "Measurement of Wall Shear Stress" in *Fluid Mechanics Measurements*, ed. by Richard J. Goldstein, Taylor & Francis, Bristol, Pennsylvania, 1996, pp. 590–611.

14. Bellhouse, B.J. and D.L. Schultz, "Determination of mean and dynamic skin friction, separation and transition in low-speed flow with a thin-film heated element," *Journal of Fluid Mechanics*, vol. 24, pt. 2, 1966, pp. 379–400.

15. Noffz, Gregory K. and Adrienne S. Lavine, "Finite Element Studies of Hot-Films for Skin-Friction Measurement," *Proceedings of the 5th ASME/JSME Joint Thermal Engineering Conference*, AJTE99-6147, San Diego, California, March 1999.

16. Liang, P.W. and K.D. Cole, "Transient Conjugated Heat Transfer From a Rectangular Hot Film," *Journal of Thermophysics and Heat Transfer*, vol. 6, no. 2, April–June 1992, pp. 349–355.

17. Chiles, Harry R., *The Design and Use of a Temperature-Compensated Hot-Film Anemometer System for Boundary-Layer Flow Transition Detection on Supersonic Aircraft*, NASA TM 100421, May 1988.

18. Soeder, Ronald H., *NASA Lewis 8- By 6-Foot Supersonic Wind Tunnel User Manual*, NASA TM 105771, Feb. 1993.

19. Hakkinen, Raimo J., Jeremy S. Neubauer, Philip J. Hamory, Trong T. Bui, and Gregory K. Noffz, "Exploratory Calibration of Adjustable-Protrusion Surface-Obstacle (APSO) Skin Friction Vector Gage," *41st Aerospace Sciences Meeting and Exhibit*, AIAA 2003-0740, Reno, Nevada, Jan. 6–9, 2003.

20. Bui, Trong T., David L. Oates, and Jose C. Gonsalez, *Design and Evaluation of a New Boundary-Layer Rake for Flight Testing*, NASA TM-2000-209014, Jan. 2000.

21. Bradshaw, P. and K. Unsworth, "Comment on 'Evaluation of Preston Tube Calibration Equations in Supersonic Flow,'" *AIAA Journal*, vol. 12, no. 9, Sept. 1974, pp. 1293–1296.

REPORT DOCUMENTATION PAGE

Form Approved
OMB No. 0704-0188

1. AGENCY USE ONLY (Leave blank)	2. REPORT DATE	3. REPORT TYPE AND DATES COVERED
	March 2003	Technical Memorandum

4. TITLE AND SUBTITLE

Experimental Evaluation of Hot Films on Ceramic Substrates for Skin-Friction Measurement

5. FUNDING NUMBERS

WU 710 55 04 SE RR 00 FTT

6. AUTHOR(S)

Gregory K. Noffz, Adrienne S. Lavine, and Philip J. Hamory

7. PERFORMING ORGANIZATION NAME(S) AND ADDRESS(ES)

NASA Dryden Flight Research Center
P.O. Box 273
Edwards, California 93523-0273

8. PERFORMING ORGANIZATION REPORT NUMBER

H-2517

9. SPONSORING/MONITORING AGENCY NAME(S) AND ADDRESS(ES)

National Aeronautics and Space Administration
Washington, DC 20546-0001

10. SPONSORING/MONITORING AGENCY REPORT NUMBER

NASA/TM-2003-210742

11. SUPPLEMENTARY NOTES

Also presented at the 6th ASME-JSME Thermal Engineering Joint Conference, Hawaii Island, Hawaii, March 16–20, 2003.

12a. DISTRIBUTION/AVAILABILITY STATEMENT

Unclassified—Unlimited
Subject Category 34

This report is available at http://www.dfrc.nasa.gov/DTRS/

12b. DISTRIBUTION CODE

13. ABSTRACT (Maximum 200 words)

An investigation has been performed on the use of low-thermal conductivity, ceramic substrates for hot films intended to measure skin friction. Hot films were deposited on two types of ceramic substrates. Four hot films used composite-ceramic substrates with subsurface thermocouples (TCs), and two hot films were deposited on thin Macor® substrates. All six sensors were tested side by side in the wall of the NASA Glenn Research Center 8-ft by 6-ft Supersonic Wind Tunnel (SWT). Data were obtained from zero flow to Mach 1.98 in air. Control measurements were made with three Preston tubes and two boundary-layer rakes. The tests were repeated at two different hot film power levels. All hot films and subsurface TCs functioned throughout the three days of testing. At zero flow, the films on the high-thermal conductivity Macor® substrates required approximately twice the power as those on the composite-ceramic substrates. Skin-friction results were consistent with the control measurements. Estimates of the conduction heat losses were made using the embedded TCs but were hampered by variability in coating thicknesses and TC locations.

14. SUBJECT TERMS

Ceramic substrates, Hot film, Hot film calibration, Hot film substrates, Skin friction

15. NUMBER OF PAGES

25

16. PRICE CODE

A03

17. SECURITY CLASSIFICATION OF REPORT	18. SECURITY CLASSIFICATION OF THIS PAGE	19. SECURITY CLASSIFICATION OF ABSTRACT	20. LIMITATION OF ABSTRACT
Unclassified	Unclassified	Unclassified	Unlimited